Contactless attitude control of an uncooperative satellite by laser ablation

Sakai, Daisuke
Kyushu University

Yoshimura, Yasuhiro
Kyushu University

Hanada, Toshiya
Kyushu University

Itaya, Yuki
SKY Perfect JSAT Corporation

他

出版情報：Acta Astronautica. 196, pp.275-281, 2022-07. Elsevier
バージョン：
権利関係：

Contactless Attitude Control of an Uncooperative Satellite by Laser Ablation

Daisuke Sakai[a], Yasuhiro Yoshimura[a], Toshiya Hanada[a], Yuki Itaya[b], Tadanori Fukushima[b]

[a]*Kyushu University, 744 Motooka, Nishi-ku, Fukuoka, 819-0395, Japan*
[b]*SKY Perfect JSAT Corporation, 8-1 Akasaka 1-chome, Minato-ku, Tokyo 107-0052, Japan*

Abstract

An active debris removal method using a laser is a promising technology for its advantage in contactless operations. This paper deals with the attitude control of an uncooperative target by a laser, which is an important phase before deorbiting. The difficulty of attitude control by the laser stems from the torque directional constraint because the laser generates thrust along the normal vector of the irradiated face irrespective of the irradiating direction. Thus, the control torque along the normal vector cannot be generated, which makes the attitude control with the laser torque challenging. To tackle this problem, this paper first designs a reference controller that assumes arbitrary control torques are available. Then, a method for determining the irradiating point is proposed so that the difference between the reference torque and the actual one is minimized. Although the proposed controller does not guarantee theoretical convergence to the desired attitude, the effectiveness of the proposed controller is numerically verified for a box-type object. Furthermore, the robustness to the uncertainties of thrust magnitude and direction is also examined by Monte Carlo simulations.

Preprint submitted to Acta Astronautica *August 22, 2022*

Keywords: Space Debris, Laser Ablation, Attitude Control, Active Debris Removal

1. Introduction

The dramatic increase of space debris in near-Earth orbit is a threat to satellite operation, and active debris removal (ADR) has been intensively studied in recent years. ADR is a promising technology in which multiple spacecraft operations are required. ADR methods using robotic arms [1, 2], nets [3], or electrodynamic tethers [4] have been proposed, which require contact operations. Such contact operations may have potential risks to the collision between a removal satellite and the target. Moreover, flexible cables such as nets or tethers have complicated dynamics, making the analysis and planning of ADR missions difficult. On the other hand, ADR methods using a laser [5, 6, 7], ion beam [8, 9], thruster plume [10], and electrostatic force [11, 12] have an advantage in contactless operations. The ADR by a laser has a lower risk of functional loss of the removal satellite due to accidental collisions.

For an effective deorbit, the thrust forces by a laser or thrust plume must be generated in a desired direction, and the rotational motion of the target should be stabilized in advance. To this end, attitude stabilization methods using contactless external forces have been studied. Vetrisano [13, 14] deals with laser-induced deorbit for asteroids. The mechanism of laser ablation in deorbit: the spot size varied with the relative distance and velocity between the target and the laser satellite is investigated. An effective attitude controller is proposed by assuming the shape of the asteroid to be an ellipsoid.

Kumar et al. [5] derive a control law that can be adapted to Envisat, which has a cylindrical shape. Borelli [15] has adopted the control algorithm in [5] to a box-wing type satellite considering plume impingement as a control input. Most of these methods are designed for detumbling a target object assuming the laser or thrust plume is irradiated at spatially discrete points. The irradiation point is determined so that the most desirable torques are generated on the target at each time instance. In other words, all possible irradiating points and their induced torques are calculated, and the determination method of the irradiating point is not explicitly formulated. Moreover, existing methods consider attitude stabilization, and the attitude angle control is not considered. For deorbiting by a laser, the attitude control of a target is significant for efficient deorbiting because the thrust direction due to laser ablation is perpendicular to the irradiation plane. That is, controlling the target attitude enables generating efficient $\Delta \boldsymbol{V}$ parallel to the orbit plane [16].

In this context, this paper proposes a control method to drive an uncooperative target's angular velocity and attitude angle to the desired ones by laser ablation. The difficulty of controlling the attitude with laser ablation thrust stems from the fact that ablation causes thrust along the normal vector of the irradiating point irrespective of the irradiating direction [17]. The control torque around the normal vector thus cannot be generated. Moreover, since the target is rotating and the laser can irradiate to the target's surface where the laser satellite can see, the laser ablation torque depends on the target attitude at each time instance. To tackle this problem, this paper first designs a reference controller that assumes that arbitrary control

torques are available. Then, the cross-product law to determine the irradiating point is proposed, which minimizes the difference between the reference torque and the actual one. Although the proposed controller does not guarantee theoretical convergence to the desired attitude, the effectiveness of the proposed controller is numerically verified. Furthermore, the robustness to uncertainties on thrust magnitude and direction is examined by Monte Carlo simulations.

2. Preliminaries

The equations of motion of a satellite and laser ablation model are summarized in this section. This study assumes that a laser satellite and the target satellite travel along the same circular orbit. For deorbiting the target satellite, the laser satellite should be orbiting forward of the target. The laser ablation model shows that the ablation thrust is along the negative normal direction of the irradiated face, which makes the attitude control by laser ablation challenging.

2.1. Dynamics and kinematics of a satellite

This paper uses three coordinate frames as illustrated in Fig. 1. The inertial frame $\{x, y, z\}$ has its origin at the Earth's center. The x axis is along the vernal equinox direction, the z axis is along the rotational axis of Earth, and the y axis completes the right-handed frame. The orbital frame $\{x_o, y_o, z_o\}$ has its origin at the center of mass of the target. The x_o axis lies in the outward direction from the Earth, the z_o axis is along the orbital angular momentum direction, and the y_o axis completes the right-handed frame. The body-fixed frame $\{x_b, y_b, z_b\}$ also has its origin at the center of

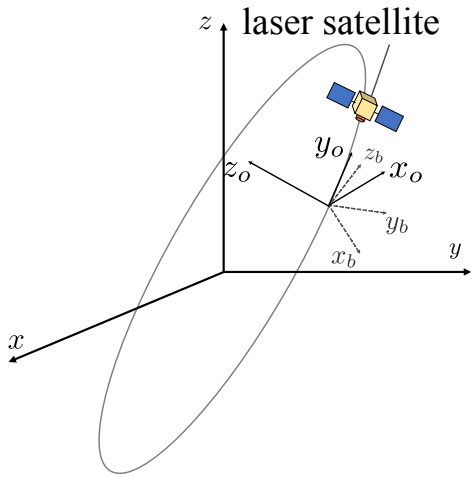

Figure 1: Inertial frame, orbital frame, and body-fixed frame.

mass of the target, and the axes are assumed to coincide with the principal axes of inertia.

The orbital motion of the target is described as

$$\ddot{\boldsymbol{r}}_{\mathrm{pos}} = -\frac{\mu}{\|\boldsymbol{r}_{\mathrm{pos}}\|^3}\boldsymbol{r}_{\mathrm{pos}} \tag{1}$$

where $\boldsymbol{r}_{\mathrm{pos}}$ is the target position in the inertial frame and μ is the Earth's gravitational constant. For simplicity, external disturbances such as atmospheric drag and solar radiation pressure are ignored in this paper.

The attitude motion of the target satellite is described with a quaternion

as

$$\dot{\boldsymbol{q}} = \frac{1}{2}\tilde{\boldsymbol{\omega}} \otimes \boldsymbol{q} \tag{2}$$

$$= \frac{1}{2}\begin{bmatrix} 0 & \omega_z & -\omega_y & \omega_x \\ -\omega_z & 0 & \omega_x & \omega_y \\ \omega_y & -\omega_x & 0 & \omega_z \\ -\omega_x & -\omega_y & -\omega_z & 0 \end{bmatrix} \boldsymbol{q} \tag{3}$$

$$J\dot{\boldsymbol{\omega}} = -\boldsymbol{\omega} \times J\boldsymbol{\omega} + \boldsymbol{\tau} \tag{4}$$

where $\boldsymbol{q} = [q_1, q_2, q_3, q_4]^T$ is the quaternion vector whose scalar part is q_4, $\boldsymbol{\omega} = [\omega_x, \omega_y, \omega_z]^T$ is the angular velocity vector in the body-fixed frame, $J = \mathrm{diag}(J_x, J_y, J_z)$ is the satellite's inertia tensor, and $\boldsymbol{\tau}$ is the control torque. In Eq. (2), $\tilde{\boldsymbol{\omega}}$ is an augmented angular velocity $\tilde{\boldsymbol{\omega}} = [\boldsymbol{\omega}^T, 0]^T$ so that the quaternion product $\otimes$ can be calculated. Note that the quaternion and the angular rate in Eqs. (3) and (4) are described with respect to the inertial frame. Since this paper uses three coordinate frames, the subscripts of the variables specify the frames. For example, $\boldsymbol{\omega}_{b/o}$ means that the angular velocity of the body-fixed frame with respect to the orbital frame.

In Section 4, the numerical simulation results are evaluated using the 3-2-1 sequence of the Euler angle (ϕ, θ, ψ). The conversion between the Euler angle and the quaternion is obtained using the following rotational matrix

from the inertial frame to the body-fixed frame.

$$R_{b/i} = \begin{bmatrix} q_1^2 - q_2^2 - q_3^2 + q_4^2 & 2(q_1q_2 + q_3q_4) & 2(q_1q_3 - q_2q_4) \\ 2(q_1q_2 - q_3q_4) & -q_1^2 + q_2^2 - q_3^2 + q_4^2 & 2(q_2q_3 + q_1q_4) \\ 2(q_1q_3 + q_2q_4) & 2(q_2q_3 - q_1q_4) & -q_1^2 - q_2^2 + q_3^2 + q_4^2 \end{bmatrix} \tag{5}$$

$$= \begin{bmatrix} \cos\theta\cos\phi & \cos\theta\sin\phi & -\sin\theta \\ \sin\theta\sin\psi\cos\phi - \cos\psi\sin\phi & \sin\theta\sin\psi\sin\phi + \cos\psi\cos\phi & \cos\theta\sin\psi \\ \sin\theta\cos\psi\cos\phi + \sin\psi\sin\phi & \sin\theta\cos\psi\sin\phi - \sin\psi\cos\phi & \cos\theta\cos\psi \end{bmatrix} \tag{6}$$

For example, the Euler angle can be obtained as

$$\tan\phi = \frac{R_{1,2}}{R_{1,1}} \tag{7}$$

$$\sin\theta = -R_{1,3} \tag{8}$$

$$\tan\psi = \frac{R_{2,3}}{R_{3,3}} \tag{9}$$

where $R_{j,k}$ means the jth row and kth column component of the rotational matrix $R_{b/i}$. Also, the following small-angle approximation can be used [18].

$$2q_1 \approx \psi \tag{10}$$

$$2q_2 \approx \theta \tag{11}$$

$$2q_3 \approx \phi \tag{12}$$

In this paper, the desired attitude and angular velocity of the target satellite is to coincide with the orbital frame. Thus, describing the quaternion and its kinematics with respect to the orbital frame is useful. Let $\boldsymbol{q}_{b/o}$ and $\boldsymbol{\omega}_{b/o}$ be the quaternion and the angular rate with respect to the orbital frame.

The kinematics is described in the same form in Eq. (2) as [19]

$$\dot{\boldsymbol{q}}_{b/o} = \frac{1}{2}\tilde{\boldsymbol{\omega}}_{b/o} \otimes \boldsymbol{q}_{b/o} \tag{13}$$

The angular velocity $\boldsymbol{\omega}_{b/o}$ has the relation $\boldsymbol{\omega}_{b/o} = \boldsymbol{\omega}_{b/i} - \boldsymbol{\omega}_{o/i}$.

2.2. Laser ablation model

The ablation model used in this paper is briefly described, and more detailed descriptions are found in [20]. When a laser lands on the surface of a target satellite, a phenomenon called ablation occurs in which the incident laser evaporates the material of the satellite body. The thrust force generated by the ablation also causes torque, which is the control input for the target attitude control in this paper.

The force generated on the target surface $\boldsymbol{f}$ is given by the product of the velocity of the ejected gas $\bar{\boldsymbol{v}}$ and the mass flow rate of the ablated material $\dot{m}$ as

$$\boldsymbol{f} = \lambda \bar{\boldsymbol{v}} \dot{m} \tag{14}$$

where λ is a constant scatter factor used to account for the non-unidirectional expansion of the ejecta gas. Figure 2 illustrates the uniform diffusion of ejecta gasses generated by laser ablation around the landing spot. Thus, the thrust force is directed in the direction of the internal normal vector of the local surface. In other words, the thrust force is always generated along the internal normal vector of the surface, which does not depend on the laser irradiation direction. This is a unique property for the system that uses laser ablation as a thrust force. Consequently, the control torque $\boldsymbol{\tau}$ by laser ablation is described with the position vector $\boldsymbol{r}$ at the laser landing point

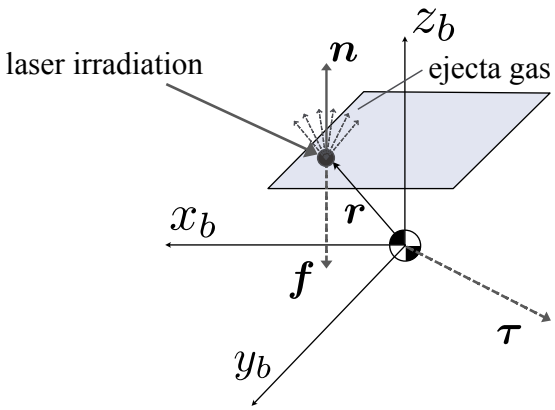

Figure 2: Geometry of the ejecta gas.

and the thrust force vector $\boldsymbol{f}$ as

$$\boldsymbol{\tau} = \boldsymbol{r} \times \boldsymbol{f} \tag{15}$$

$$= -\|\boldsymbol{f}\|\boldsymbol{r} \times \boldsymbol{n} \tag{16}$$

The ablation thrust and its torque in Eqs. (14) and (16) are ideal formulations. In practice, other factors, such as the spot size of the laser and the relative distance between the laser satellite and the target, affect the magnitude of the ablation thrust [20]. Moreover, since the thrust direction depends on the normal vector of the face, the modeling error of the target shape would yield the ablation thrust in undesired directions. This paper considers these uncertainties on the magnitude and direction of the ablation thrust in numerical examples. The magnitude uncertainty of the thrust is defined as the multiplicative uncertainty. That is, the thrust magnitude with uncertainty $\|\hat{\boldsymbol{f}}\|$ is written as

$$\|\hat{\boldsymbol{f}}\| = \eta\|\boldsymbol{f}\| \tag{17}$$

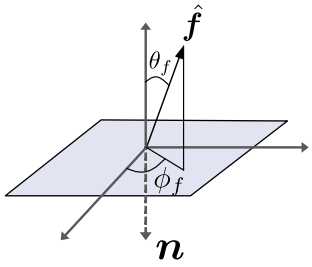

Figure 3: Thrust directional uncertainty

where η is the magnitude uncertainty coefficient and is assumed to follow the normal distribution $\mathcal{N}(m_f, \sigma_f^2)$ where m_f is the mean and σ_f^2 is the variance. Figure 3 defines the thrust force under directional uncertainty. The directional uncertainty is expressed with the angle θ_f that follows the normal distribution $\mathcal{N}(m_\theta, \sigma_\theta^2)$ and the angle ϕ_f that follows the uniform distribution from 0 to 360 deg.

3. Methodology

To tackle the input directional constraint, a reference controller based on quaternion feedback is firstly designed. Secondly, the laser irradiation point on the target surface is determined using the cross-product law as explained in Section 3.2. If the determined irradiation point would be out of the range of the target surface, the irradiation point is corrected to be within the maximum length of the target surface, which is also described in Section 3.2.

3.1. Reference controller

A reference controller is designed with a quaternion feedback controller [21]. The quaternion feedback consists of proportional and derivative parts with

respect to a desired attitude as

$$\boldsymbol{\tau}_{\mathrm{ref}} = -k_q \boldsymbol{q}_e - k_\omega \boldsymbol{\omega}_e \tag{18}$$

where $\boldsymbol{q}_e$ is the error quaternion, $\boldsymbol{\omega}_e$ is the angular velocity error, and k_q and k_ω are control gains. The error between the current attitude or angular velocity and the desired one is calculated as

$$\boldsymbol{q}_e = \boldsymbol{q}_{b/i} \otimes \boldsymbol{q}_d^{-1} \tag{19}$$

$$\boldsymbol{\omega}_e = \boldsymbol{\omega}_{b/i} - \boldsymbol{\omega}_d \tag{20}$$

where the subscript d means the desired value of the variable. This paper sets the desired attitude of the target satellite to coincide with the orbital frame, i.e., $\boldsymbol{q}_d = \boldsymbol{q}_{o/i}$ and $\boldsymbol{\omega}_d = \boldsymbol{\omega}_{o/i}$.

3.2. Cross-product-based determination of irradiation point

Although the reference controller in Eq. (18) is designed assuming that arbitrary torques can be generated, such a reference torque cannot be realized due to the directional constraint on the ablation thrust. The thrust direction depends on the normal direction of the irradiation point, and the irradiation point should be determined so that the generated torques are as close to the reference torques as possible. To this end, the following cross-product law is proposed.

$$\boldsymbol{r} = \frac{c_1}{\|\boldsymbol{f}\|^2} \left(\boldsymbol{f} \times \boldsymbol{\tau}_{\mathrm{ref}} \right) \tag{21}$$

where $\boldsymbol{r}$ is the laser irradiation position vector expressed in the body-fixed frame and c_1 is the correction coefficient of the irradiation point which is

discussed later. Using the cross-product law in Eq. (21), the actual torque generated is written as

$$\boldsymbol{\tau} = \boldsymbol{r} \times \boldsymbol{f} \tag{22}$$

$$= \frac{c_1}{\|\boldsymbol{f}\|^2} (\boldsymbol{f} \times \boldsymbol{\tau}_{\mathrm{ref}}) \times \boldsymbol{f} \tag{23}$$

$$= c_1 \boldsymbol{\tau}_{\mathrm{ref}} - c_1 \frac{\boldsymbol{\tau}_{\mathrm{ref}}^T \boldsymbol{f}}{\|\boldsymbol{f}\|^2} \boldsymbol{f} \tag{24}$$

The first term in Eq. (24) is equal to the reference torque and the second term is a disturbance torque that stems from the input directional constraint. If the reference torque is ideally perpendicular to the force direction, i.e., $\boldsymbol{\tau}_{\mathrm{ref}}^T \boldsymbol{f} = 0$, the second term vanishes and the reference torque is purely realized by the cross-product law. Such a situation, however, rarely occurs, and the second term is considered as a disturbance. Thus, the cross-product law to determine the irradiation point does not guarantee the convergence to the desired attitude. Nevertheless, because the magnitude of the ablation thrust is small and the rotational motion is periodic, the reference torque is expected to be realized averagely, even if the disturbance term exists.

The irradiation position $\boldsymbol{r}$ must be on the target's surface. Offsetting a vector in the opposite direction to the thrust force vector $\boldsymbol{f}$ is required as follows.

$$\boldsymbol{r} = \frac{c_1}{\|\boldsymbol{f}\|^2} (\boldsymbol{f} \times \boldsymbol{\tau}_{\mathrm{ref}}) + c_2 \frac{\boldsymbol{f}}{\|\boldsymbol{f}\|} \tag{25}$$

where c_2 is the offset coefficient and $c_2 = \boldsymbol{n}^T \boldsymbol{r}$ for a convex body. Note that adding the offset correction term does not affect the control torque generated because $\boldsymbol{f} \times \boldsymbol{f} = 0$. The coefficient c_1 is calculated to limit the irradiation position vector within the maximum length of the target surface.

4. Numerical examples

Numerical simulations are conducted to verify the proposed attitude controller. Four simulation conditions are examined: 1) under no thrust uncertainty, 2) under thrust magnitude uncertainty, 3) under thrust directional uncertainty, and 4) under both thrust magnitude and directional uncertainties. Although the proposed controller does not guarantee theoretical convergence, 100 Monte Carlo runs in each case are conducted for the numerical verification in this section. It is noted that the first case does not consider thrust uncertainty, and the initial attitude and angular velocity are random variables for each Monte Carlo run.

4.1. Simulation condition

The box shape and size illustrated in Fig. 4 are considered as the target configuration, and its moment of inertia is assumed to be $(J_x, J_y, J_z) = (32.6, 73.7, 79.9)$ kgm^2 assuming a 150 kg class satellite. The target and laser satellite are assumed to be in the same inclined circular orbit at an altitude of 1200 km. The inclination is 87.9 deg, and the other orbital elements such as the right ascension of the ascending node, the argument of perigee, and the argument of latitude are zero. Orbital perturbations and their torques are not considered in this paper, and these orbital elements determine the desired attitude with respect to the inertial frame. This paper focuses on the target's attitude control, and the orbital decay due to the ablation thrust is also ignored.

The initial quaternion is random and the initial angular velocity is randomly distributed with $\|\boldsymbol{\omega}_{b/i}\| = 6$ deg/s, corresponding to 1 rpm. The same

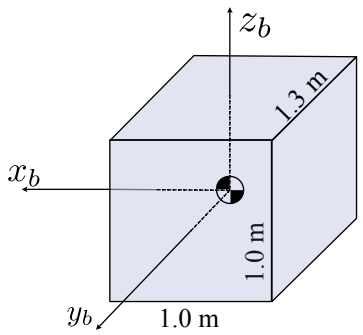

Figure 4: Box-type target

Table 1: Uncertainties

	thrust magnitude m_f, σ_f	thrust direction m_θ, σ_θ [deg]
mean	1.0	0.0
standard deviation	0.1	15.0

simulation condition is used for all four cases. The ablation thrust force is assumed to be 0.72 mN when no uncertainties exist, supposing a 20μNs/J impulse and a laser power of 1 J at 36 Hz [22]. The mean and standard deviation of the uncertainties are summarized in Table 1. It is noted again that the thrust magnitude uncertainty is multiplicative. The control gains are empirically determined and set to $k_q = 1.0 \times 10^{-3}$ and $k_\omega = 5.0 \times 10^{-2}$.

4.2. Results under no uncertainty

Figure 5 represents one of the time history of the angular rate error from 100 Monte Carlo runs, where the initial condition is $\boldsymbol{q}_{b/i} = [0, 0, 0, 1]^T$ and $\boldsymbol{\omega}_{b/i} = [3.00, -3.00, 4.24]^T$ deg/s in this case. The angular rate errors about all three axes converge to zero, which means that the angular velocity $\boldsymbol{\omega}_{b/i}$

corresponds to the orbital angular rate $\boldsymbol{\omega}_{o/i}$. Figure 6 shows the time history of the Euler angle with a 3-2-1 sequence (ϕ, θ, ψ) for better understanding. The attitude is also controlled to the desired one, but θ has slow convergence. This is because the attitude is controlled to make the body-fixed frame correspond to the orbital frame, and in this situation, the laser satellite orbiting forward can irradiate $+y_b$ face of the target alone. That is, the ablation thrust causes along the y_b axis, and the attitude angle around the y_b axis is almost uncontrollable. The attitude angle around the y_b axis, however, can gradually converge because of the coupling between the orbit and attitude motion.

In all Monte Carlo runs, the target attitude is successfully controlled. Table 2 summarizes the mean and standard deviation of the residual attitude angle error and the angular rate error for 100 Monte Carlo runs. It is noted that these values are calculated for the final time step of all Monte Carlo runs and not averaged over time. The attitude angle error in Table 2 is also described with the 3-2-1 Euler angle. Although the attitude angle around the y_b axis, θ, has the largest mean error and standard deviation, the other attitude angles have the mean and standard deviation less than 1 deg. The mean and standard deviation of the angular rate error also have small errors, which verifies the effectiveness of the proposed controller.

4.3. Results with thrust magnitude uncertainty

Figures 7 and 8 describe the time histories of the angular velocity error and the Euler angle error under the thrust magnitude uncertainty, respectively. The initial attitude and angular rate are the same as the simulation in Figs. 5 and 6. Both the angular rate error and attitude error converge

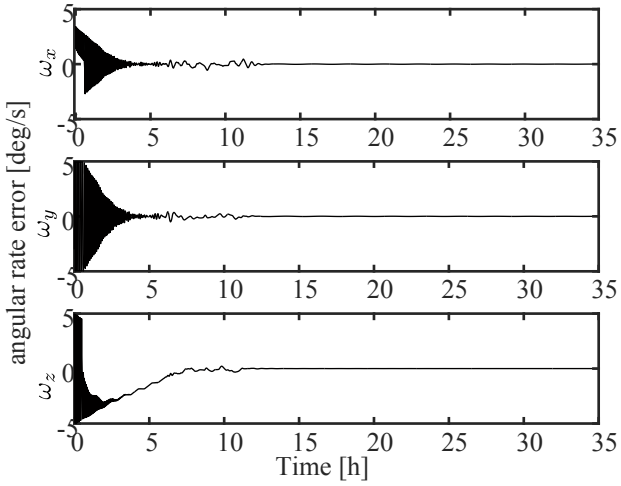

Figure 5: Time history of the angular rate error under no uncertainty

Table 2: Monte Carlo simulation results under no uncertainty

	Euler angle error ϕ, θ, ψ [deg]	Angular rate error $\boldsymbol{\omega}_{e,b/i}$ [deg/s]
mean	0.7939, 4.3637, 0.3791	0.0049, 0.0038, 0.0005
standard deviation	0.1953, 5.1217, 0.5414	0.0037, 0.0028, 0.0013

to zero and mean that the target attitude is successfully controlled even if the ablation thrust has uncertainty in the thrust magnitude. Compared to Fig. 6, the attitude convergence time in Fig. 8 is almost the same even under uncertainty. The target attitude is successfully controlled in all Monte Carlo runs. Table 3 describes the mean and standard deviation of the attitude angle error and angular rate error. The attitude control accuracy is almost same as the result in Table 2 and has the small mean error and standard deviation. This result means that the uncertainty on the thrust magnitude

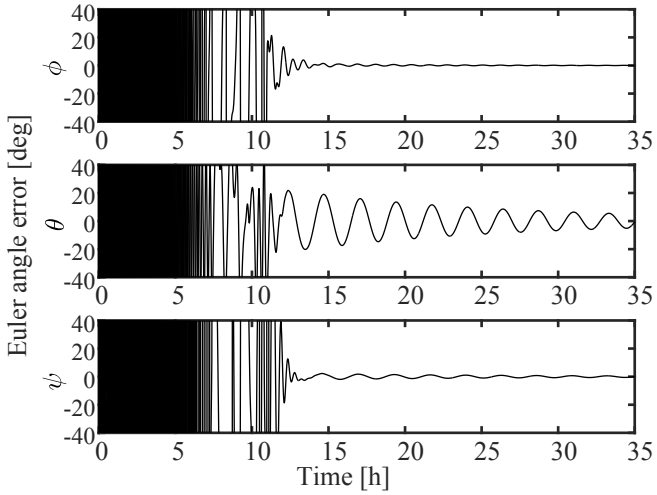

Figure 6: Time history of the Euler angle error under no uncertainty

Table 3: Monte Carlo simulation results with thrust magnitude uncertainty

	Euler angle error ϕ, θ, ψ [deg]	Angular rate error $\boldsymbol{\omega}_{e,b/i}$ [deg/s]
mean	0.1796, 4.7668, 0.4708	0.0046, 0.0036, 0.0006
standard deviation	0.6613, 3.9575, 0.3837	0.0034, 0.0028, 0.0022

does not degrade the accuracy of the attitude control.

4.4. Results with thrust directional uncertainty

Figures 9 and 10 represent the time histories of the angular velocity error and the Euler angle error under the thrust directional uncertainty, respectively. The initial attitude and angular rate are also the same as in the previous simulation. The target attitude is controlled to the desired one under the uncertainty on the thrust direction. The attitude convergence time

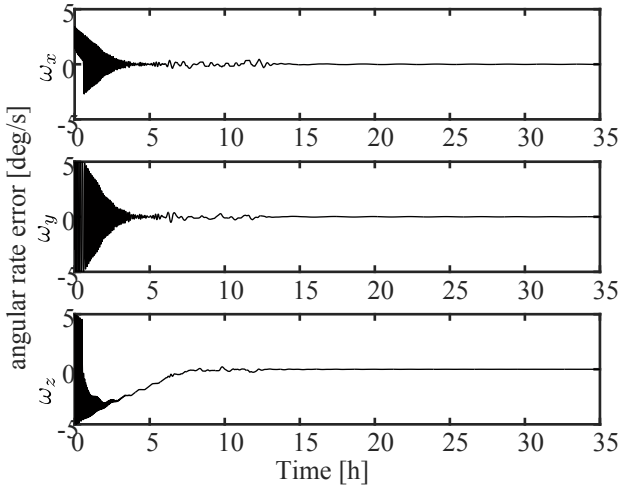

Figure 7: Time history of the angular rate error under thrust magnitude uncertainty

in Fig. 10 is almost the same as the one shown in Fig. 6. The results from 98 Monte Carlo runs indicate the convergence of the target attitude and only two runs show the attitude divergence. Table 4 describes the mean and standard deviation of the attitude angle error and angular rate error. The attitude angle θ has a larger mean error compared to the previous two cases. The standard deviations also have larger values, which indicate that the thrust directional uncertainty impacts the attitude control accuracy more than the uncertainty on the thrust magnitude.

4.5. Results with thrust magnitude and directional uncertainties

Figures 11 and 12 respectively show the time histories of the angular velocity error and the Euler angle error under both the thrust magnitude and directional uncertainties. The initial attitude is the same as in the previous cases. Even if there are combined uncertainties in thrust magnitude and direction, the proposed controller can drive the target attitude to the desired

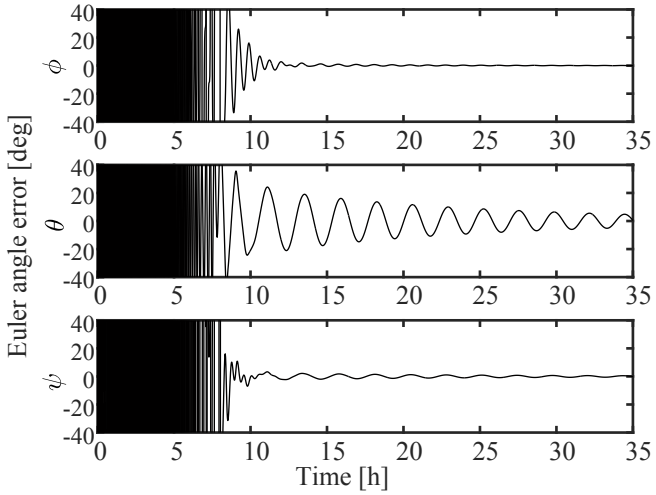

Figure 8: Time history of the Euler angle error under thrust magnitude uncertainty

Table 4: Monte Carlo simulation results with thrust directional uncertainty

	Euler angle error ϕ, θ, ψ [deg]	Angular rate error $\boldsymbol{\omega}_{e,b/i}$ [deg/s]
mean	0.3481, 5.8038, 0.6489	0.0056, 0.0043, 0.0008
standard deviation	1.0955, 4.8929, 0.6176	0.0047, 0.0034, 0.0020

one. However, the attitude convergence time in Fig. 12 is the longest, which is a reasonable result due to uncertainties. Only two Monte Carlo runs show the attitude divergence, and the other 98 runs indicate the convergence of the target attitude. The mean and standard deviation of the attitude angle error and angular rate error are tabulated in Table 5. The standard deviation of both the attitude error and angular rate error have the largest value compared to the other cases. This result indicates that, although the accuracy of the

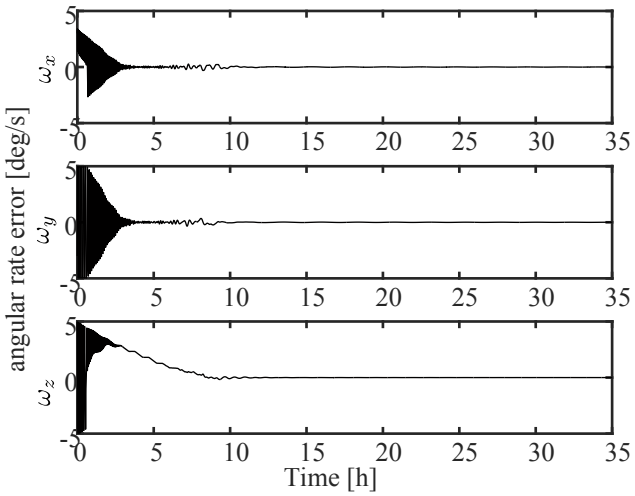

Figure 9: Time history of the angular rate error under thrust directional uncertainty

attitude control is degraded, the robustness of the proposed controller is useful for practical mission situations under the thrust uncertainties.

5. Conclusions

This paper deals with the attitude control of an uncooperative target by laser ablation thrust. Because the ablation thrust is generated along the

Table 5: Monte Carlo simulation results with thrust magnitude and directional uncertainties

	Euler angle error ϕ, θ, ψ [deg]	Angular rate error $\boldsymbol{\omega}_{e,b/i}$ [deg/s]
mean	0.5236, 4.1946, 0.5852	0.0052, 0.0046, 0.0010
standard deviation	2.9810, 4.9346, 0.9467	0.0072, 0.0050, 0.0047

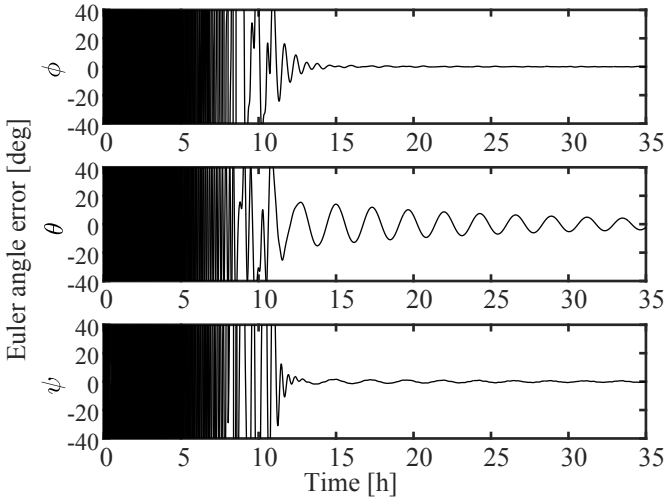

Figure 10: Time history of the Euler angle error under thrust directional uncertainty

normal direction of the irradiating point, the attitude control torque direction is constrained regardless of the irradiating direction. To tackle this difficulty, the reference controller is designed using quaternion feedback, and the method of determining the irradiating point is proposed, minimizing the difference between the reference torque and the actual torque generated. Numerical simulations with 100 Monte Carlo runs verify the effectiveness of the proposed controller. Furthermore, its robustness to the uncertainties on the thrust magnitude and direction is examined in the Monte Carlo simulations, which indicates that the thrust directional uncertainty impacts the attitude control accuracy more than the uncertainty on the thrust magnitude.

References

[1] S. Nishida, S. Kawamoto, Y. Okawa, F. Terui, S. Kitamura, Space debris removal system using a small satellite, Acta Astronautica 65

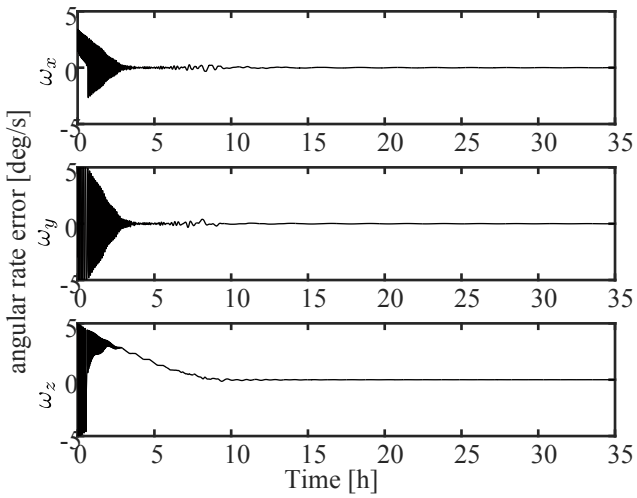

Figure 11: Time history of the angular rate error under thrust magnitude and directional uncertainties

(2009) 95–102.

[2] S. Nishida, S. Kawamoto, Strategy for capturing of a tumbling space debris, Acta Astronautica 68 (2011) 113–120.

[3] M. Shan, J. Guo, E. Gill, Contact dynamic models of space debris capturing using a net, Acta Astronautica 158 (2019) 198–205.

[4] S. Kawamoto, Y. Ohkawa, S. Kitamura, S.-i. Nishida, Strategy for active debris removal using electrodynamic tether, Transactions of the Japan Society for Aeronautical and Space Sciences, Space Technology Japan 7 (2009) Pr_2_7–Pr_2_12.

[5] R. Kumar, R. J. Sedwick, Despinning orbital debris before docking using laser ablation, Journal of Spacecraft and Rockets 52 (2015) 1129–1134.

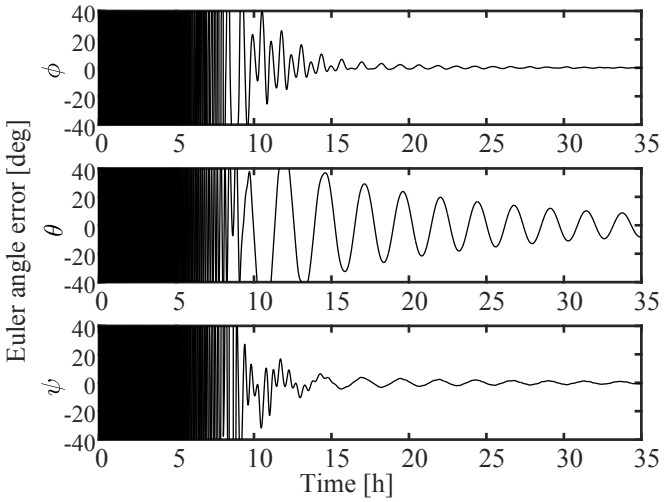

Figure 12: Time history of the Euler angle error under thrust magnitude and directional uncertainties

[6] Y. Matsushita, Y. Yoshimura, T. Hanada, Y. Itaya, T. Fukushima, Risk assessment of a large constellation of satellites in low-earth orbit, TRANSACTIONS OF THE JAPAN SOCIETY FOR AERONAUTICAL AND SPACE SCIENCES, AEROSPACE TECHNOLOGY JAPAN 20 (2022) 10–15.

[7] S. Fukii, D. Sakai, Y. Yoshimura, Y. Matsushita, T. Hanada, Y. Itaya, T. Fukushima, Assessing collision probability in low-thrust deorbit, Journal of Space Safety Engineering (2022).

[8] V. S. Aslanov, A. S. Ledkov, Attitude motion of cylindrical space debris during its removal by ion beam, Mathematical Problems in Engineering 2017 (2017) 1–7.

[9] V. S. Aslanov, A. S. Ledkov, V. G. Petukhov, Spatial dynamics and

attitude control during contactless ion beam transportation, Journal of Guidance, Control, and Dynamics (2021) 1–6.

[10] Y. Nakajima, H. Tani, T. Yamamoto, N. Murakami, S. Mitani, K. Yamanaka, Contactless space debris detumbling: A database approach based on computational fluid dynamics, Journal of Guidance, Control, and Dynamics 41 (2018) 1906–1918.

[11] T. Bennett, H. Schaub, Contactless electrostatic detumbling of axisymmetric geo objects with nominal pushing or pulling, Advances in Space Research 62 (2018) 2977–2987.

[12] Detumbling an uncontrolled satellite with contactless force by using an eddy current brake, volume 2013 IEEE/RSJ International Conference on Intelligent Robots and Systems, IEEE, 2013.

[13] M. Vetrisano, N. Thiry, M. Vasile, Detumbling large space debris via laser ablation, in: Detumbling large space debris via laser ablation, volume 2015 IEEE Aerospace Conference, IEEE, 2015, pp. 1–10.

[14] M. Vetrisano, C. Colombo, M. Vasile, Asteroid rotation and orbit control via laser ablation, Advances in Space Research 57 (2016) 1762–1782.

[15] G. Borelli, G. Gaias, C. Colombo, Rotational control with plume impingement to aid rigid capture of an uncooperative failed satellite, in: 2020 AAS/AIAA Astrodynamics Specialist Conference, American Institute of Aeronautics and Astronautics (AIAA), 2020.

[16] T. Fukushima, D. Hirata, K. Adachi, Y. Itaya, J. Yamada, K. Tsuno, T. Ogawa, N. Saito, M. Sakashita, S. Wada, End of life deorbit service

with a pulsed laser onboard a small satellite, in: Proceedings of the 8th European Conference on Space Debris, 2021.

[17] H. Chang, X. Jin, W. Zhou, Experimental investigation of plume expansion dynamics of nanosecond laser ablated al with small incident angle, Optik 125 (2014) 2923–2926.

[18] J. L. Crassidis, J. L. Junkins, Optimal estimation of dynamic systems, Chapman and Hall/CRC, 2004.

[19] F. Celani, Quaternion versus rotation matrix feedback for spacecraft attitude stabilization using magnetorquers, Aerospace 9 (2022) 24.

[20] M. Vasile, A. Gibbings, I. Watson, J.-M. Hopkins, Improved laser ablation model for asteroid deflection, Acta Astronautica 103 (2014) 382–394.

[21] B. Wie, P. M. Barba, Quaternion feedback for spacecraft large angle maneuvers, Journal of Guidance, Control, and Dynamics 8 (1985) 360–365.

[22] K. Tsuno, S. Wada, T. Ogawa, T. Ebisuzaki, T. Fukushima, D. Hirata, J. Yamada, Y. Itaya, Impulse measurement of laser induced ablation in a vacuum., Opt Express 28 (2020) 25723–25729.